Inductive coupling in IP measurements and applications to 3D distributed array field data inversion

Leif H. Cox*, TechnoImaging; Michael S. Zhdanov, TechnoImaging and the University of Utah; and Fouzan Alfouzan, King Abdulaziz City for Science and Technology

SUMMARY

Modern distributed DC/IP survey arrays can collect large amounts of broadband electrical data. These arrays are no longer limited to simple in-line dipole-dipole or pole-pole surveys as they were in the past. This allows geophysicists to apply true 3D geometries and use arbitrary transmitter and receiver positions, which opens the door to high resolution 3D information about the spectral complex resistivity response of the earth and possibly mineral discrimination. However, these arrays also increase the computational complexity of solving the inverse problem for earth's parameters. In addition, the increase in the frequency range of the collected data along with the complex wire paths raises the chances of incurring inductive coupling, which can hide the complex resistivity response. This paper examines the problems of inductive coupling in broadband, complex wire path surveys and finds that it can indeed affect the IP response. By using the full EM solution and known geometry of the wire paths, we can increase the usable IP data by about one decade of frequency or time measurements. We have modified an existing modeling and inversion code to handle the explicit geometry of the wire paths and to include the full EM effects, all in an efficient manner, which makes it possible to conduct a rigorous inversion of these 3D survey data. An inversion of the field data compares well with other information, demonstrating the effectiveness of the developed method.

INTRODUCTION

Resistivity-induced polarization (DC/IP) surveys are typically applied to collect data about the earth's resistivity at the DC limit and chargeability. Surveys have been designed to maximize the collection of resistivity and IP data while minimizing the electromagnetic induction effects, often referred to as inductive coupling (IC).

Spectral IP methods can be used not only for mineral detection, but they open the door for possible mineral discrimination (Pelton et al., 1978; Zhdanov, 2008; Zhdanov et. Al., 2018c). To do this, broadband complex resistivity information about the earth's response must be collected and analyzed. The collection of true broadband spectral IP data requires higher frequencies or early times, which increases the chances of incurring coupling. Additionally, as surveys become more complex and truly 3D, it is more difficult to eliminate the IC effect.

The inductive coupling response can be larger than the IP response and it has been a major hindrance in the past to interpretation (e.g., Wynn and Zonge, 1977). The IC effect has been examined several times before, mostly in the context of standard array configuration (e.g., Dey and Morrison, 1973). It

has also been attempted to remove the IC effects and to correct the data to pure IP and resistivity responses (e.g., Routh and Oldenburg, 2001).

In this paper, we look at the effects of inductive coupling and advanced survey designs in the context of extracting spectral IP information. We examine the effects of resolving both the chargeability and time constant of a medium in the presence of inductive coupling with modern 3D geometries. We develop an efficient method and computer code to invert 3D spectral IP data collected in Saudi Arabia during the Glass Earth Pilot Project (Zhdanov et. al. 2019). We use an integral equation forward modeling scheme, which includes full 3D EM effects and the geometry of all wire paths, for forward modeling. The earth is represented as voxels with the complex conductivity of each voxel being parameterized into the GEMTIP model. We solve for the four dominate GEMTIP parameters for each voxel. The results of the inversion of the field SIP data helped to improve the subsurface images of the mineralized target in the survey area.

Field survey layout

To give the impetus for the modeling section, we first show the field survey layout (Figure 1) to which we will apply the new inversion code. There are 9 transmitter dipoles operated in the case; each neighboring current electrode pair operated as a current bipole. The voltage at each receiver point is measured in reference to a common ground. By using this setup, only one common receiver wire needs to be used for all receiver locations, greatly simplifying survey logistics and increasing the data collection speed. Each receiver can be referenced to every other receiver in the processing to create a large number of receiver dipoles. However, this produces long receiver wire paths, some of which run parallel to transmitter current dipoles, and hence inductive coupling can become problematic if not modeled correctly.

MODELING

We begin with the simple case of a polarizable half-space for simplicity in developing some intuition about the IP and IC problems across a variety of source-receiver geometries and time and frequencies. The transmitter wire is modeled as a series of electric dipoles on the surface of the homogeneous earth and integrated with Gaussian quadrature. The receiver wires are modeled by integrating the electric field along the wire path (equation (1)) from receiver electrode M to electrode N to synthesize the voltage difference which would be measured in the field:

$$\Delta V_{MN} = \int_{M}^{N} \mathbf{E} \cdot \mathbf{dl}. \tag{1}$$
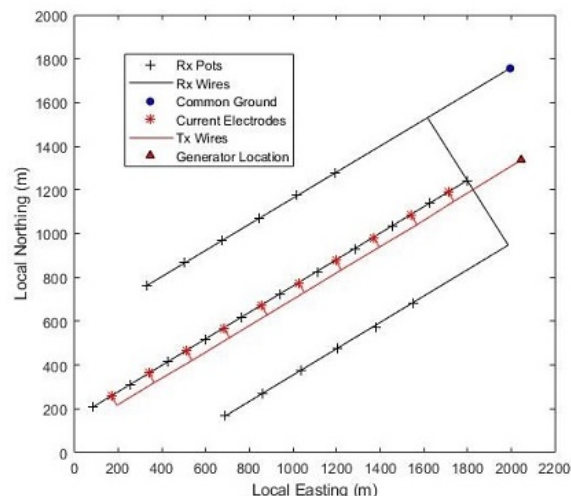
Figure 1: Field survey layout.

We consider first a simple case of a half-space characterized by the Cole-Cole model parameters listed in Table 1. The current is 1 A. The time domain response is computed by using a cosine transform of the imaginary part of the frequency domain spectrum, which gives the step-off response. Note that an infinite step-off is used for these calculations for simplicity, but using a 50% duty cycle repeating waveform of limited bandwidth allows us to draw the same conclusions, and the true waveform is used for the field data inversion. Also note that the time range and frequency range shown here is greater than available commercial systems, but it is instructive to look at the expanded spectrum.

Table 1: Base Cole-Cole model parameters for half-space IC testing.

Parameter	Value
DC Resistivity (ρ_{DC})	100 [Ohm-m]
Chargeability (η)	100 [mV/V]
Time Constant (τ)	0.1 [s]
Relaxation Factor (C)	0.5 []

To isolate the effects of the inductive coupling and wire path, we compute four different responses for each. One is the true response which includes all effects, as would be measured in the field. This includes the electromagnetic inductive response (IC), the true wire path, and the complex conductivity of the earth. The other three responses are a straight wire path from the M to N receiver electrode positions (ignoring the true wire path), DC approximation (ignoring IC), and ignoring induced polarization. Note that in the case of the DC approximation, the wire path does not matter, as the fields are conservative, and the line integral in equation (1) is path independent.

We show an example of the severe inductive coupling effects in Figure 2. This shows the the frequency domain apparent resistivity and phase as functions of frequency, and time domain voltage and apparent chargeability. There are several features

to point out in this figure. Panel (a) shows that the DC approximation is excellent to around 1 Hz, at which IC begins to dominate. Panel (b) shows the frequency domain quadrature response. As one should expect, the phase reflects both the polarization and IC much more stronger than the in-phase response. With this configuration, the IC dominates the phase for nearly the entire frequency range. Only at the very lowest frequencies ($< 3x10^{-4}$Hz) does the IP effect the response. Above this frequency, IC effects completely dominate the spectrum. This frequency is well below the range of commercial systems. In the time domain (panels (d) and (e)) the IC part completely dominates from the earliest times to 5ms. By 50ms, the response is free of inductive coupling and only the IP decay remains.

Modeling shows that, as expected, longer offsets, receiver wire paths which traverse close to the transmitter dipoles, and more conductive media all increase the effects of the IC, both by increasing the amplitude and pushing the domination to later times or lower frequencies.
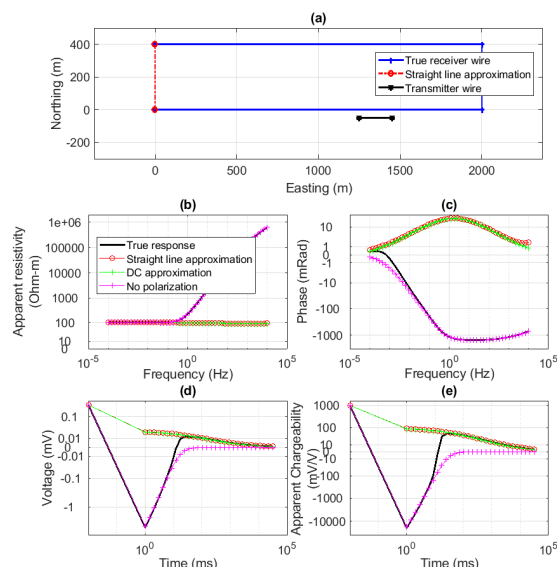

Figure 2: Frequency and time domain response with a non-conventional survey layout. Panel (a) shows the source-receiver layout. Note that, only active wires paths are shown and modeled. Panel (b) presents the frequency domain apparent resistivity. Panel (c) shows the frequency domain phase response. Panel (d) displays the time domain voltage decay. Panel (e) shows the apparent chargeability. The first tic on the time domain curve is the on-time channel.

Discrimination of the polarization time constant when considering IC effects

The goal of collecting the spectral IP data is in measuring the details about the polarization spectrum of the medium. Real rocks exhibit time constants that range for many orders of magnitude (Burtman and Zhdanov, 2015; Burtman et. al., 2014), while many time domain surveys measure less than two decades

of decay (e.g., 100 ms to 2 s). Additionally, inductive coupling can dominate the early times and higher frequencies, so this leads to the question if a reasonable range of time constants of the media can be determined from the real data.
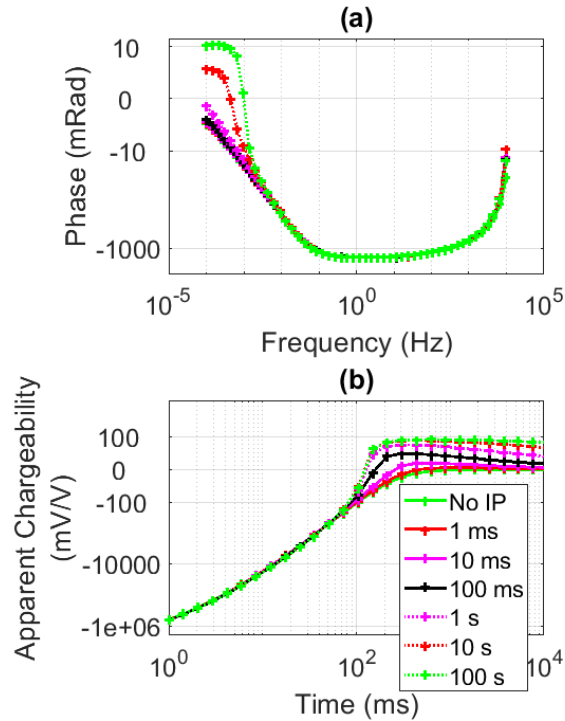

Figure 3: Variation of response with time constants. Panel (a) shows the frequency domain response and panel (b) the time domain response. The time constant for each response is shown in the legend. One can see the dominating inductive response earlier than 100 ms and continuing effects to several 100s of ms.

Figure 3 shows the response of the halfspace given in Table I with the survey configuration shown in Figure 2. Only the true wire path with full EM effects have been computed. Each curve shows a different time constant of the medium. These vary from 1 ms to 100 s, quite a wide and realistic range. Also shown is a case with no chargeability. Note that for the frequency domain, there is no separation of the curves at frequencies above 1 mHz, which indicates the time constant for this configuration would not be resolved in the frequency domain using conventional frequency ranges. In the time domain, there is separation of the curves for time constants from around 10ms to 10s. This occurs over the time window from 100 ms to 10 s. Outside of this range the time constant cannot be resolved. Longer time constants would require lower base frequencies, and resolving shorter time constants require accounting for the inductive coupling.

Discussion of IC effects

The frequency domain response has a much larger contribution from IC than time domain. The time domain shows bet-

ter sensitivity to IP and time constants. The wire path is less important in time domain modeling but can still have a large effect when transmitter receiver separations are large and the medium is conductive (< 100 Ohm-m).

In both frequency domain and time domain, there is about one decade of time or frequency response that contains information from both IC and IP. This means that by including wires paths and the full EM solution, we can extract IP information from the response one decade earlier than if the DC approximation is used. This is especially important when short time constants are expected.

INVERSION

We use the modeling and inversion methods of Zhdanov et al (2018c) with the modification that we include full receiver wire paths (the cited paper had included transmitter wire paths already). As shown in Figure 1, with a distributed array such as this, the wire lengths can become long when two referenced receivers are not on the same line. One must be careful when modeling surveys of this type, because inductive coupling can be a dominate effect.

The voltage response is given by:

$$\Delta V_{M_k M_l}^b(\omega) = \sum_{p=k}^{l-1} \int_{M_p}^{M^{p+1}} \mathbf{E}(r', \omega) \cdot \mathbf{dl} \qquad (2)$$

and the sensitivities are given by:

$$\frac{\partial \Delta V_{M_k M_l}(\omega)}{\partial \sigma_i} = \sum_{p=k}^{l-1} \int_{M_p}^{M^{p+1}} \left(\iiint_{D_i} \mathbf{G_E}(r', r_i, \omega) \mathbf{E}(r_i, \omega) dV \right) \cdot \mathbf{dl}$$
$$(3)$$

where p is the dummy index of the receiver wire segment end points, the prime indicates a position along the receiver wire path, the dl is the receiver wire path (electrodes or bends).

FIELD DATA INVERSION

The inversion was run with horizontal cell sizes of 50 m x 50 m. There were 8 cells in the z direction varying from 26 to 223 m in thickness giving a total depth range of 0 to 600 m. There were 9 transmitters and 23 receiver electrodes for total of 482 combinations and these each had 21 time channels from 40 ms to 1.92 s plus the on-time channel. The center line had the 9 transmitters (see Figure 1) which were 200 m dipoles. The receivers were combinations of electrodes from all three receiver lines. The receiver lines were 350 m apart and approximately 3 km long.

We have applied the developed inversion code to these field SIP data. The inversion converged to a final χ^2 misfit of 0.7 from the starting misfit of 4.4. The error model used for the observed data is given by the following equation:

$$\varepsilon_i = |d_i| \cdot 10\% + 3x10^{-4}V \qquad (4)$$

where $|d_i|$ is the absolute value of the ith data point. The data weights are the inverse values of these errors.

There is no standard plotting conversion for this type of distributed array data. We are plotting the physical fields to develop some intuition about the processes and to visually compare the observed and predicted data to analyze the data fit. Each image shows the voltage corresponding to one transmitter position. The plotting point is the average position of the two potential measurement points, as was shown in the synthetic example. Figure 4 show examples of the data fit for different transmitters and time channels. The observed and predicted data visually match very well.
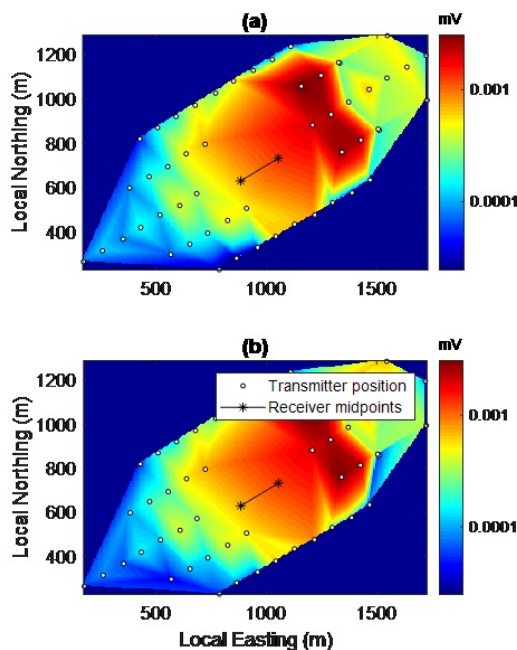

Figure 4: Plot of observed (a) and predicted (b) data for transmitter number 5 and a mid-time channel.

The inversion results under the transmitter line is shown in Figure 5. The results match well with other geophysics and the data fit is within the error level of the data.

CONCLUSIONS

We have developed a SIP inversion method and code which take into account all inductive coupling, the wires paths, and includes IP effects through the use of the GEMTIP model. We examined the cases where the wire paths and inductive effects were important and confirmed that the time domain data are much better than the frequency domain to measure SIP parameters. For arbitrary 3D arrays, we found that for half spaces with resistivity above 100 Ohm-m and for typical sampling times (50 ms after turn off), the inductive effects do not play a large role. However, to recover the earlier times, for more conductive medium, or for longer offsets (> 1 km) when the
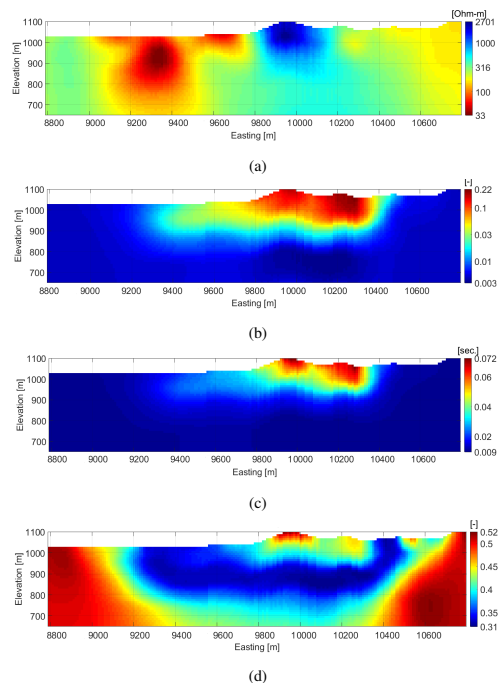

Figure 5: Inversion results under the center line of the 3D array. Panel (a) shows the resistivity, panel (b) shows the chargeability, panel (c) the recovered time constant, and panel (d) the relaxation parameter.

receiver wire is close to the transmitter, the inductive effects do need to be included in the inversion.

The interpretation of the field SIP data was based on the new method, and it recovered a resistivity model which closely matched independently recovered resistivity models obtained previously from different data sets.

The new developed method of 3D inversion of the distributed SIP survey data can handle any type of arbitrary receiver and transmitter array for any frequency or time domain surveys. The use of the integral equation method and conjugate gradient optimization scheme with a novel approach to computing sensitivities via wire segments make this new method and code efficient for the large field surveys.

ACKNOWLEDGMENTS

REFERENCES

Burtman, V., H. Fu, and M. Zhdanov, 2014, Experimental study of induced polarization effect in unconventional reservoir rocks: Geomaterials, **4**, 117–128, doi: https://doi.org/10.4236/gm.2014.44012.

Burtman, V., and M. S. Zhdanov, 2015, Induced polarization effect in reservoir rocks and its modeling based on generalized effective-medium theory: Resource-Efficient Technologies, **1**, 34–48, doi: https://doi.org/10.1016/j.reffit.2015.06.008.

Commer, M., G. Newman, K. Williams, and S. Hubbard, 2011, 3D induced-polarization data inversion for complex resistivity: Geophysics, **76**, no. 3, F157–F171, doi: https://doi.org/10.1190/1.3560156.

Dey, A., and H. Morrison, 1973, Electromagnetic coupling in frequency and time-domain induced-polarization survey over a multilayered earth: Geophysics, **38**, 380–405, doi: https://doi.org/10.1190/1.1440348.

Pelton, W. H., S. H. Ward, P. G. Hallof, W. R. Sill, and P. H. Nelson, 1978, Mineral discrimination and removal of inductive coupling with multi-frequency IP: Geophysics, **43**, 388–609.

Routh, P. S., and D. W. Oldenburg, 2001, Electromagnetic coupling in frequency-domain induced polarization data: A method for removal: Geophysical Journal International, **145**, 59–76, doi: https://doi.org/10.1111/j.1365-246X.2001.00384.x.

Rudd, J., and G. Chubak, 2017, The Facility of a Fully-Distributed DCIP System with CVR: 15th SAGA Biennial Conference and Exhibition.

Wynn, J. C., and K. L. Zonge, 1977, Electromagnetic coupling: Geophysical Prospecting, **25**, 29–51.

Xu, Z., and M. S. Zhdanov, 2015, Three-Dimensional Cole-Cole Model Inversion of Induced Polarization Data Based on Regularized Conjugate Gradient Method: IEEE Geoscience and Remote Sensing Letters, **12**, 2311–2315, doi: https://doi.org/10.1109/LGRS.2015.2474744.

Yoshioka, K., and M. S. Zhdanov, 2005, Three-dimensional nonlinear regularized inversion of the induced polarization data based on the Cole - Cole model: Physics of the Earth and Planetary Interiors, **150**, 29–43, doi: https://doi.org/10.1016/j.pepi.2004.08.034.

Zhdanov, M., 2008, Generalized effective-medium theory of induced polarization: Geophysics, **73**, no. 5, F197–F211, doi: https://doi.org/10.1190/1.2973462.

Zhdanov, M. S., 2002, Geophysical Inverse Theory and Regularization Problems: Elsevier.

Zhdanov, M. S., 2018, Foundations of Geophysical Electromagnetic Theory and Methods: Elsevier.

Zhdanov, M. S., F. A. Alfouzan, L. Cox, A. Alotaibi, M. Alyousif, D. Sunwall, and M. Endo, 2018a, Large-Scale 3D Modeling and Inversion of Multiphysics Airborne Geophysical Data: A Case Study from the Arabian Shield, Saudi Arabia: Minerals, **8**, 271, doi: https://doi.org/10.3390/min8070271.

Zhdanov, M. S., V. Burtman, M. Endo, and W. Lin, 2018b, Complex resistivity of mineral rocks in the context of the generalized effective medium theory of the induced polarization effect: Geophysical Prospecting, **66**, 798–817, doi: https://doi.org/10.1111/1365-2478.12581.

Zhdanov, M. S., M. Endo, L. H. Cox, and D. A. Sunwall, 2018c, Effective-medium inversion of induced polarization data for mineral exploration and mineral discrimination: Case study for the copper deposit in Mongolia: Minerals, **8**, 28, doi: https://doi.org/10.3390/min8010028.